3D finite element modeling of the blow molding process

Cédric Champin, Michel Bellet, Fabrice Schmidt, Jean François Agassant, Yannick Le Maoult, G. Denis

3D FINITE ELEMENT MODELING OF THE STRETCH BLOW MOLDING PROCESS

Paper n° 148

C. Champin (a,b,c), M. Bellet (a), F.M. Schmidt (b), J.-F. Agassant (a), Y. Le Maoult (b), G. Denis (c).

(a) CEMEF, Ecole des Mines de Paris, BP 207, 06904 Sophia-Antipolis Cedex, France.
(b) CROMeP, Ecole des Mines d'Albi Carmaux, Campus Jarlard, 81013 Albi Cedex 09, France.
(c) NESTLE Waters MT, BP 101, 88 804 Vittel Cedex, France.

Cedric.champin@ensmp.fr

Abstract

The stretch blow molding process of PET bottles is a two-step process. First, a cold tube-shape preform is heated using an infrared oven above PET glass transition temperature (about 80°C) in order to reach the forming temperature. The softened preform is then simultaneously stretched and inflated with a rod and air pressure. The final wall thickness of the bottle is both related to heating parameters as well as stretch blow molding ones. It leads to a complex thermo-mechanical problem for which specific numerical models must be developed. In this work, a complete 3D finite element modeling of the stretch blow molding process has been developed including both infrared heating and forming steps.

The energy transfer between the infrared oven and the irradiative surface of the preform is modeled using a ray tracing method. In the same time, the amount of radiation intensity absorbed by the polymer is approximated with a Rosseland model. Owing to that, the radiation heat transfer results in a pure conductive heat transfer. All the thermal computations will be compared to the so-called PLASTIRAD control volume software [MON2001] and to a temperature analytical model.

Considering the deformation step, a Mooney-Rivlin hyperelastic model has been implemented in Forge3® software in order to account for the PET rheological behavior. The numerical model is developed using a velocity pressure formulation and P1+/P1 tetrahedral finite elements. In order to validate the hyperelastic behavior, computations are compared to a Mooney-Rivlin analytical model of a free inflation tube. This model enables to obtain the tube internal radius versus a given pressure on the internal surface.

I- Introduction

The injection stretch-blow molding process is the most widely used in the P.E.T bottle production [ROS1989]. This process is segmented in two main stages. First, a cold preform is heated in an infrared oven above glass transition temperature (80°C for P.E.T.). Then, the softened preform is inflated and stretched with assistance of a rod in a mold which has the shape of the desired bottle (cf. figure 1). The performance of P.E.T. bottles so-produced depends on many variables including the initial preform shape and several process parameters. It is well-known that these having major impact on mechanical properties are the initial preform temperature and the bi-axial elongation rates.

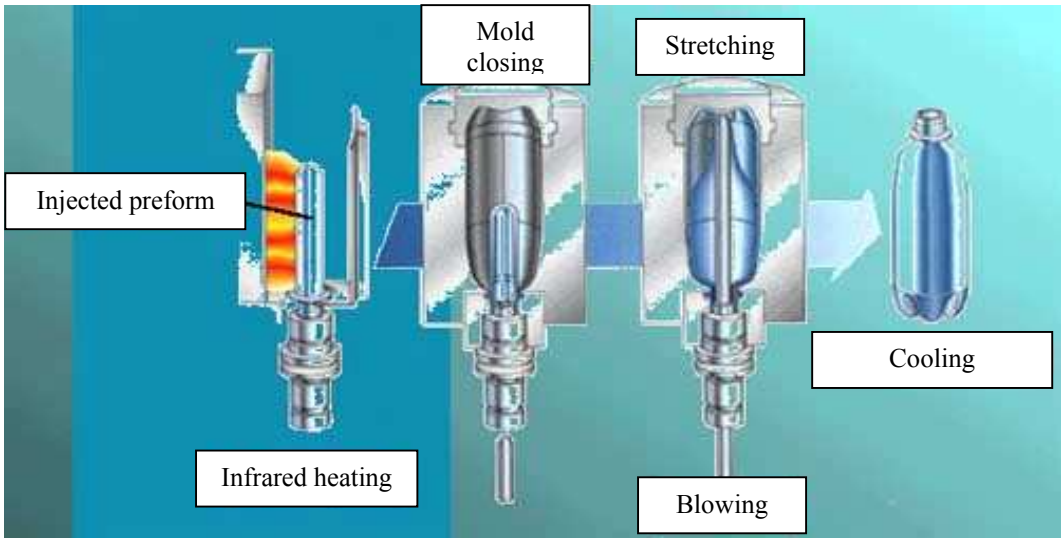

Figure 1 : Scheme of the injection blow molding process.

Since last decade, the reduction of weight became one of the main demands for the design of packaging. Therefore, process optimizing tends more and more to produce bottles of minimum thickness having the best mechanical properties. But mechanical properties of bottles also depend in turn on final thickness distribution and P.E.T. strain hardening resulting from stretching. In consequence, optimizing the process becomes a huge task when only based on experimental studies. For that reason, several numerical simulations for stretch-blow molding process optimization have been developed to save time and provide more understanding of the process. However, in order to be accurate enough, the simulation necessitates a 3D numerical model taking into account both the heating and inflation stages.

As illustrated in figure 2 a typical infrared oven is constituted of a row of halogen tube lamps which allows a rapid heating (about 30 seconds), two kinds of reflectors (back and front of preform) and a cooling fan. The cooling fan is necessary to insure that the external preform surface does not burn but also to prevent surface temperature preform exceeding P.E.T. thermal crystallization temperature (about 135°C). The preforms are transported across the oven while they rotate continuously. The rotation allows to obtain an homogeneous temperature distribution in the angular direction. The threaded portion of the preform is protected by a heat shield in order to avoid heating. Once warmed, the preform exits from the oven and is allowed to thermally equilibrate before being placed in the stretch-blow mold. Thus, there are several processing parameters to set (heating time, equilibrium time, rotation speed, heat transfer coefficient,...) in order to heat conditioning preforms.

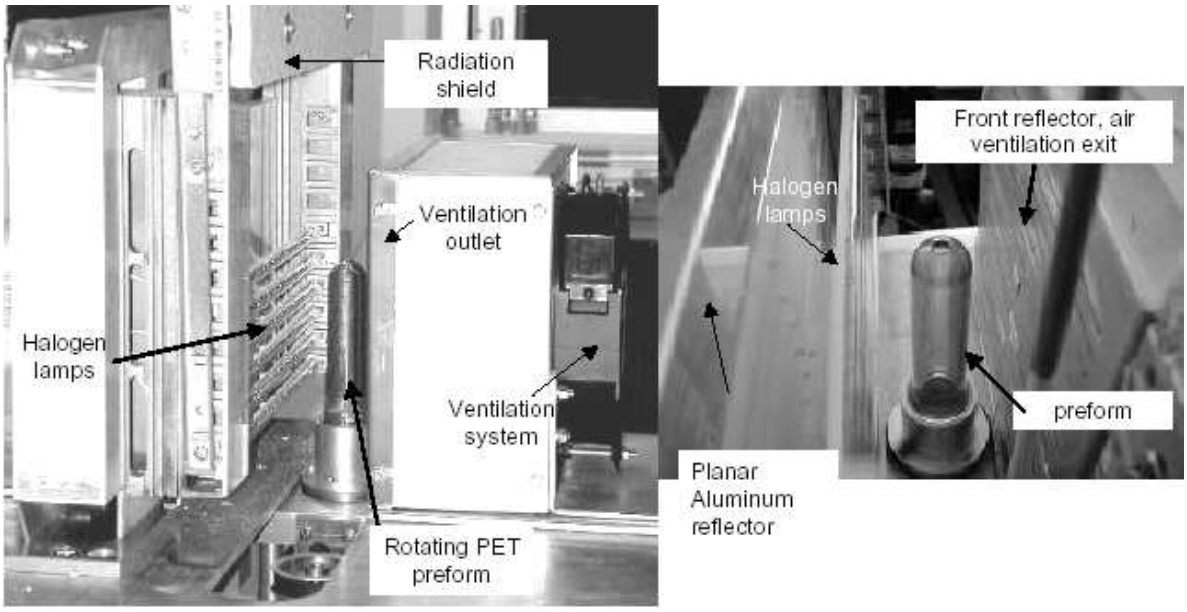

Figure 2 : Infrared heating experimental set-up.

A few models of the heat transfer inside an infrared oven have been developed. In 1992, Lebaudy [LEB1992] has developed a two-dimensional finite difference model in which the radiation flux is assumed to be uniform along the preform height. The value of the heat transfer coefficient between the air and the polymer is assumed to be constant to account for the air forced convection due to the cooling fan. Shelby [SHE1991] employed a simple numerical approach to determine the effect of infrared lamp temperature on reheat rate of PET. Radiative heat transfer was assumed. The methodology predicted the transient one-dimensional temperature distribution. DiRaddo et al [DIR1993] proposed a two-dimensional approach using the finite element method where the fraction of energy leaving the heaters surface arriving at the preform surface (i.e. the view factor) is estimated analytically. Hartwig [HAR1996] in his model includes the back and front reflectors and the complex displacement of the preform (translation and rotation). Venkateswaran et al [VEN1997] use an analytical approach to calculate the view factors too.

The blowing step has been equally the object of a lot of research this last two decades. 2D viscoelastic model [SCH1992] has allowed to understand the complex thermo mechanical problem implemented. Rapidly, some studies have been specifically focused on the PET behavior heated up to its glass transition temperature. Thus, the Institute of Physical and Chemical of Research (RIKEN) programmed a 3D shell finite element software using a viscoplastic behavior law [WAN1998]. But major part of the works have shown that this behavior was more hyperelastic than viscoelastic, and as a result, numerical model must be developed using Mooney-Rivlin or neo-Hookean potentials. Thus, the Santa Clara University (SCUDC) developed a software using membrane elements with a Lagrangian formulation and a Mooney-Rivlin potential. The Queen's University of Belfast programmed a special Abaqus version dedicated to the blow molding simulation. It used Mooney-Rivlin, Ogden and more interesting, Buckley hyperelastic law [MEN2000]. Recently, Gorlier [GOR2001] or Marco [MAR2003] noted correlations between the Edwards Vilgis potential [EDW1986] and the deformation of PET subjected to multi-axial loads. Moreover, for a numerical point of view, the thin shell models proved their limits for the mechanical as for the thermal problem, regarding the more and more complex bottle shapes.

As a consequence, the two steps of the stretch blow molding process will be 3D modeled in this work, with a finite element method implemented in the Forge3® commercial software. First, a modeling approach capable of predicting the three-dimensional transient temperature profile in the preform during the conditioning station (reheating and equilibrating) is presented. Conduction and radiation heat transfer modes have to be taken into account. The mechanical problem is considered using a hyperelastic Mooney-Rivlin law implemented with a velocity/pressure formulation and remeshing phases during the calculations, if necessary.

II- Infrared heating model

In its classical form, the heat balance equation can be written :

$$\rho c_p \frac{dT}{dt} = \nabla \cdot (k \nabla T) - \nabla \cdot \left(\overrightarrow{q_r}\right) \qquad [1]$$

where $\overrightarrow{q_r}$ is the radiation heat flux
(cf. nomenclature)

Using the following boundary conditions :

- $T(x,O) = T_0$ on Ω, initial temperature
- $\overrightarrow{q_r}.\vec{n} = \phi_{imp}$ on $\partial\Omega_{flux}$,
  ϕ_{imp} an imposed heat flux
- $(k \nabla T).\vec{n} = h_{conv}(T - T_{ext})$ on $\partial\Omega_{conv}$,
  for heat convection

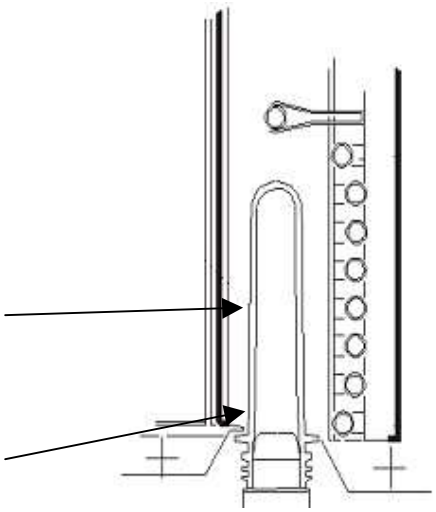

Figure 3 : Infrared heating of the perform.

Rosseland has developed a diffusion approximation of the radiation heat transfer in the case of large optical thickness [MOD1993]. This kind of approximation has been widely used for glass forming processes [LIN2002]. Numerical simulation using this method speeds up, because the radiation heat transfer is solved using a conductive heat transfer form. Thus, the radiation heat flux reduces to :

$$\nabla \cdot \left(\overrightarrow{q_r}\right) = -\nabla \cdot \left[\left(\frac{16 \sigma_{SB}}{3 k_{ROSS}(T)} T^3 \right) \vec{\nabla}(T) \right] \text{ where } \frac{1}{k_{ROSS}(T)} = \frac{\int_0^\infty \frac{1}{\kappa_\nu} \frac{dB(T,\nu)}{dT} d\nu}{\int_0^\infty \frac{dB(T,\nu)}{dT} d\nu} \qquad [2]$$

We have implemented this method in Forge3® in order to test the accuracy of this approximation. This software is based on the Galerkin weak formulation. As a consequence, the heat balance equation can be reformulated in a matrix form :

$$[C]\frac{dT}{dt} + [K]T = [Q] \quad [3]$$

which is solved by a diagonal preconditioned conjugate gradient method. For more details, one can refer to [MAR1997].

The validation case is a semi infinite sheet in P.E.T. heated with a constant heat flux ϕ_{imp} of 20 000 W/m² (about three ovens with for each seven lamps) on its front face (fig. 4).

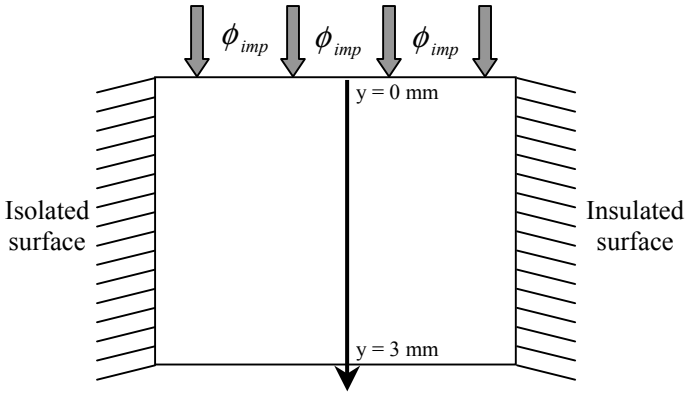

Figure 4 : Semi infinite sheet heated by a constant heat flux.

Taking into account the thermal conductivity and radiation absorption using Beer Lambert law [4], an analytical expression for temperature [5] can be calculated [MON2001] :

$$\phi = \phi_{imp} e^{-\kappa y} \qquad [4]$$

$$T(y,t) = T(y,t=0) - \frac{\phi_{imp} e^{-\kappa y}}{k\kappa^2} + \frac{\phi_{imp}}{k\kappa} 2\sqrt{\alpha_d t}\left[ierfc\left(\frac{y}{2\sqrt{\alpha_d t}} \right)\right] \qquad [5]$$

$$+ \frac{\phi_{imp}}{2k\kappa^2} e^{\kappa^2 \alpha_d t + \kappa y}\left[erf\left(\kappa\sqrt{\alpha_d t} + \frac{y}{2\sqrt{\alpha_d t}} \right)\right] + \frac{\phi_{imp}}{2k\kappa^2} e^{\kappa^2 \alpha_d t - \kappa y}\left[erf\left(\kappa\sqrt{\alpha_d t} - \frac{y}{2\sqrt{\alpha_d t}} \right)\right]$$

Numerical simulations have been performed using the mesh in figure 5 where every lateral faces were considered as adiabatic. The mesh has 786 nodes, 3377 elements and the CPU time was less than one minute. The PET thermal properties are referenced below [MON2001] :

$k = 0.29\ Wm^{-1}K^{-1}$ $\qquad \kappa = 1900\ m^{-1}$ $\qquad \alpha_d = 1.17\ 10^{-7}\ m^2 s^{-1}$

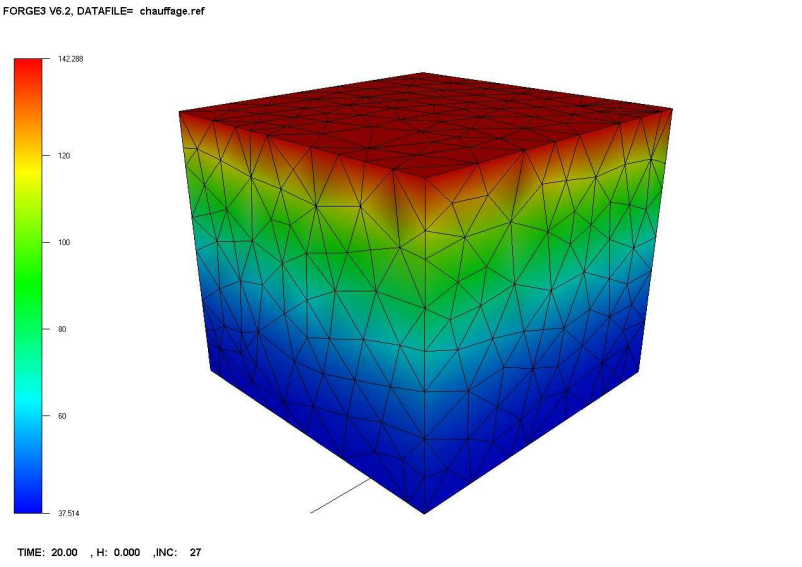

Figure 5 : Mesh used for the temperature calculation (°C).

In figure 6, the temperature evolution for the analytical case and numerical one are plotted. The temperature computed on the front face is greater than the analytical one (maximum of 40%). This difference is due to the fact that the analytical model takes into account the radiative absorption (Beer-Lambert law) in the temperature calculation, whereas in the same time, the numerical model (i.e. the Rosseland approximation) assumes an equivalent conductivity representing only 1.5% of the thermal conductivity of the P.E.T. Consequently, the heat flux imposed on the front face is not diffused in the sheet thickness, but in a very thin layer (k_{ROSS} , and so the optical thickness is about 150 µm).

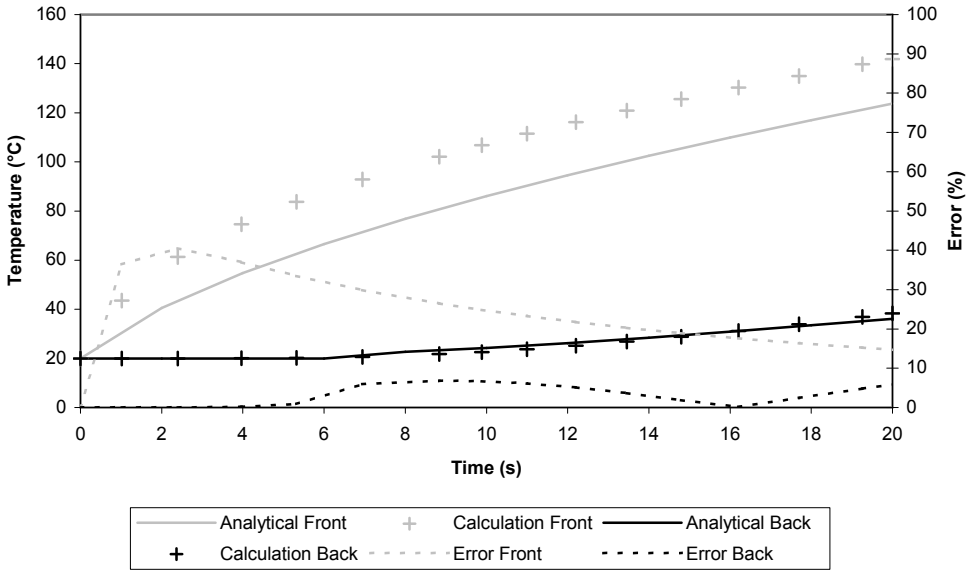

Figure 6 : Evolution of temperature in polyethylene sheet.

This comparison demonstrates the necessity to develop a new method in order to solve radiation heat transfer. Thus, a ray tracing method has been implemented to improve the numerical model. As a preliminary result (fig. 7), this technique allows us to compute the view factors between a preform and a punctual source.

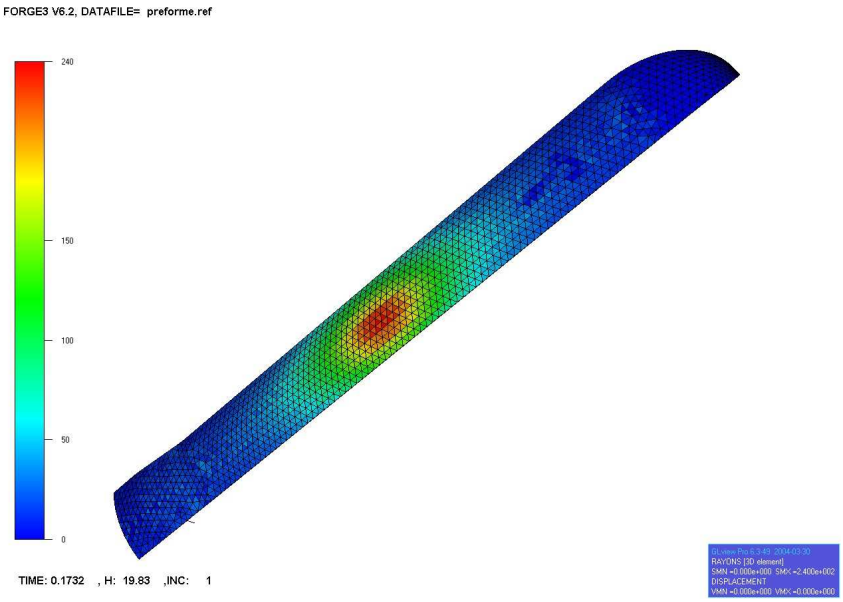

Figure 7 : Distribution of the rays emitted by a punctual source.

III- Mechanical model

As Gorlier [GOR2001] showed in his PhD, the PET is assumed to have a hyperelastic rheological behavior above its glass transition temperature. This is characterized by the existence of a deformation energy W function of the transformation gradient tensor $\underline{\underline{F}}$. The classical relationship for the Cauchy stress tensor versus W if we consider PET as an incompressible material is [GER1973] :

$$\underline{\underline{\sigma}} = -p' \underline{\underline{I}} + 2\frac{\partial W}{\partial I_1}\underline{\underline{B}} - 2\frac{\partial W}{\partial I_2}\underline{\underline{B}}^{-1} \qquad [6]$$

In a first approach to our study, the Mooney-Rivlin potential has been chosen for its simplicity and its capacity to model the PET behavior :

$$W = C\left[(I_1 - 3) + \alpha(I_2 - 3)\right] \qquad [7]$$

Finally, the stress tensor is obtained by :

$$\underline{\underline{\sigma}} = -p' \underline{\underline{I}} + 2C\underline{\underline{B}} - 2C\alpha\underline{\underline{B}}^{-1} = -p' \underline{\underline{I}} + \underline{\underline{\sigma}}' \qquad [8]$$

This rheological model has been integrated into Forge3® using a velocity/pressure updated Lagrangian formulation together with tetrahedral elements. The Galerkin method could be written, neglecting gravity and inertia contributions :

$$\int_{\partial\Omega} \underline{S} \cdot \underline{v}^* dS - \int_{\Omega} \underline{\underline{\sigma}} : \underline{\underline{\dot{\varepsilon}}}^* dV = \qquad [9]$$

with $\underline{v}^*$ a virtual velocity field.

This formulation is discretized in space using P1+ / P1 tetrahedral finite elements. This element allows to calculate the velocity and the pressure in each node additional velocity degrees of freedom ("bubble" type degrees of freedom that are interpolated linearly in the four sub tetrahedral (fig.8)) in the middle of the element.

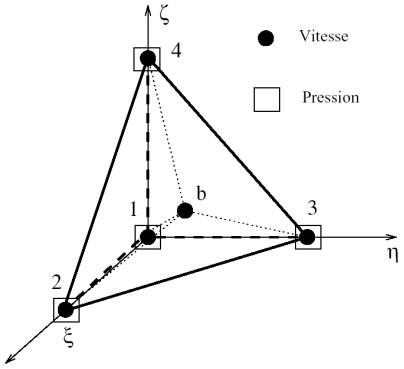

Figure 8 : P1+/P1 element.

In this case, the Galerkin method gives a second equation in the case of the bubble and finally, a third one for the incompressibility assumption

$$\int_{\Omega} p'^* div(v + b) dV = 0 \qquad [10]$$

with v the node velocity and b the bubble one.

The discretization of [9] results in a non linear set of equations, the unknown of which are the nodal velocity field and the nodal pressure field. This set of equations is solved by a Newton-Raphson method, requiring an analytical form of the tangent matrix.

$$\frac{\partial \sigma'^{\,t+\Delta t}_{kj}(v)}{\partial v_{ml}} = 2C\Delta t \,\frac{\partial N_m}{\partial x^0_p}\left(\delta_{lk}F^{t+\Delta t}_{jp} + \delta_{lj}F^{t+\Delta t}_{kp}\right) - C\alpha\Delta t\varepsilon^2_{pfq}\varepsilon_{krs}\varepsilon_{jrs}F^{t+\Delta t}_{fr}F^{t+\Delta t}_{qs}\left(\frac{\partial N_m}{\partial x^0_r}\delta_{lf}F^{t+\Delta t}_{qs} + F^{t+\Delta t}_{fr}\frac{\partial N_m}{\partial x^0_s}\delta_{lq}\right) \quad [12]$$

$\underline{\underline{F}}$ is then computed using the following relationship :

$$F_{ij} = \left(\frac{\partial N_m}{\partial \xi_k}X^m_{oi}\right)^{-1}\frac{\partial N_n}{\partial \xi_k}X^n_i \quad [13]$$

This formulation will be the basis of all the future development to solve the system.

For the validation, an analytical solution has been developed in order to assess the numerical model. An axi-symmetrical thick tube is inflated using an imposed internal pressure (fig. 9). The lower and upper pressure transverse sections of the tube are supposed to remain in fixed horizontal planes (in other words, the height of the tube section is fixed). The polymeric tube is assumed to have a Mooney-Rivlin behavior.

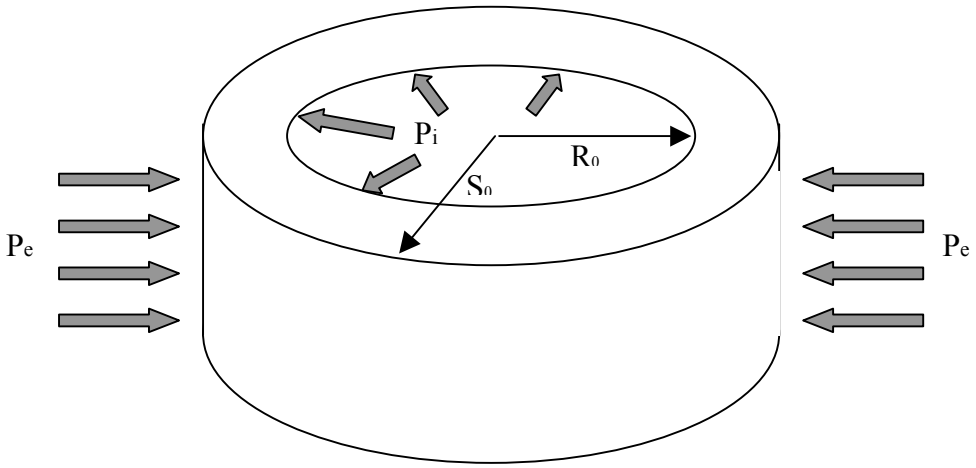

Figure 9 : Hyperelastic tube inflation.

The following relationship exists between the radial coordinate R at current time t and R_o the initial one t = 0 [SCH2000] :

$$r^2 - R^2 = r_o^2 - R_o^2 \quad \Rightarrow \quad r = \sqrt{r_o^2 - R_o^2 + R^2} \qquad [14]$$

Deriving [14], we calculate the gradient tensor $\underline{\underline{F}}$ [15] and then the Cauchy stress tensor $\underline{\underline{\sigma}}$.

$$F_{rr} = \frac{\partial r}{\partial r_o} = \frac{r_o}{r} \qquad [15]$$

Using the pressure boundary conditions, this leads to

$$\frac{\Delta P(t)}{C(1+\alpha)} = \frac{S_o^2}{R^2 + S_o^2 - R_o^2} - \frac{R_o^2}{R^2} + \ln\left(\frac{S_o^2}{R_o^2}\frac{R^2}{R^2 + S_o^2 - R_o^2}\right) \qquad [16]$$

where $\Delta P(t) = p_i - p_e$ and S is the external radius at current time t.

This analytical model enables to obtain the internal radius versus the pressure.

The numerical computations have been processed using the following boundary conditions:

- neo-Hookean hyperelastic behavior (i.e. $\alpha = 0\ MPa$ et $C = 1\ MPa$),
- an inflation pressure is applied on the internal surface of the tube with a linear variation from 0 MPa at 0 second to 0.6 MPa at 1 second,
- the initial mesh has 42 nodes and 101 elements (figure 10),
- the initial internal radius is 5mm and the initial thickness is 2mm.

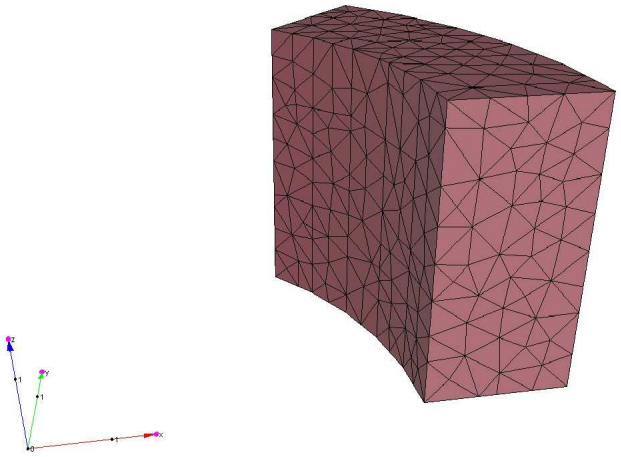

Figure 10 : Section of inflation tube mesh.

In figure 11, both numerical and analytical internal radius versus pressure are plotted as well as error. The agreement is good (maximum error 4%).

$$Error = \left|\frac{R_{Analytical} - R_{Calculation}}{R_{Analytical}}\right| \cdot 100$$

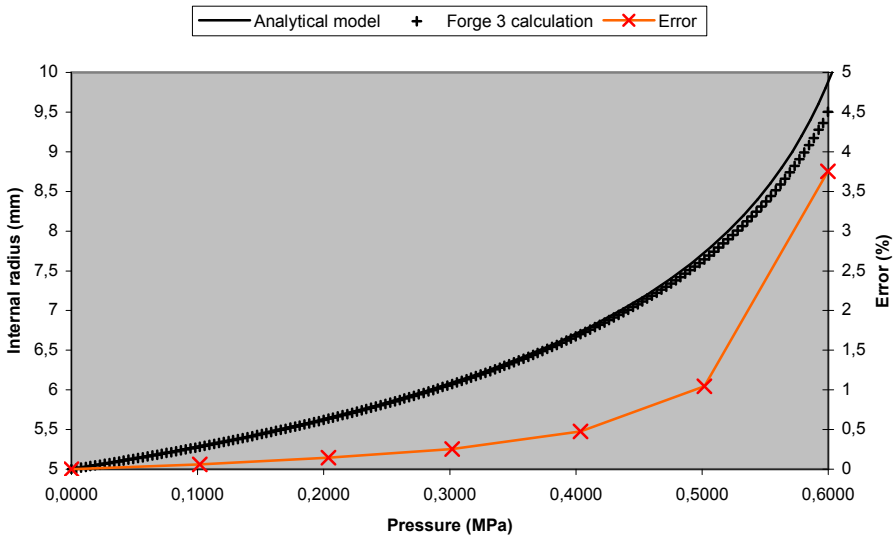

Figure 11 : Internal radius variation versus pressure.

IV- Blow molding computations

In a preliminary computation, an isothermal free inflation simulation of a preform has been performed using a neo-Hookean behavior. The parameters used for this calculations have been referenced in Table 1 and the mesh preform in figure 12.

Neo-Hookean parameters	$C = 1\ MPa$ $\alpha = 0\ MPa$
Set pressure	Linear $t = 0\ s \rightarrow P = 0\ MPa$ $t = 0.8\ s \rightarrow P = 0.8\ MPa$
Preform dimensions	Thickness $= 3\ mm$ Internal radius $= 10\ mm$ Length $= 101\ mm$

Table 1 : Calculations parameters.

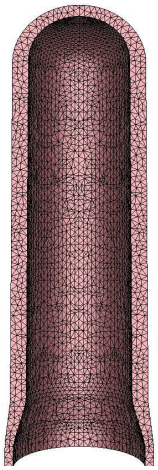

Figure 12 : Mesh of the preform
(44 403 nodes, 223 155 elements).

As a first result (fig. 13), this calculations took a long time to be achieved but allowed finally to obtain a good result. Moreover, the relaxation phase due to the hyperelastic behavior could be checked numerically. Indeed, if the pressure applied inside the preform decreases to zero, then, the preform relaxes to its initial shape. The shape of the preform during free inflation will be soon compared with experimental measured realized using a fast CCD camera.

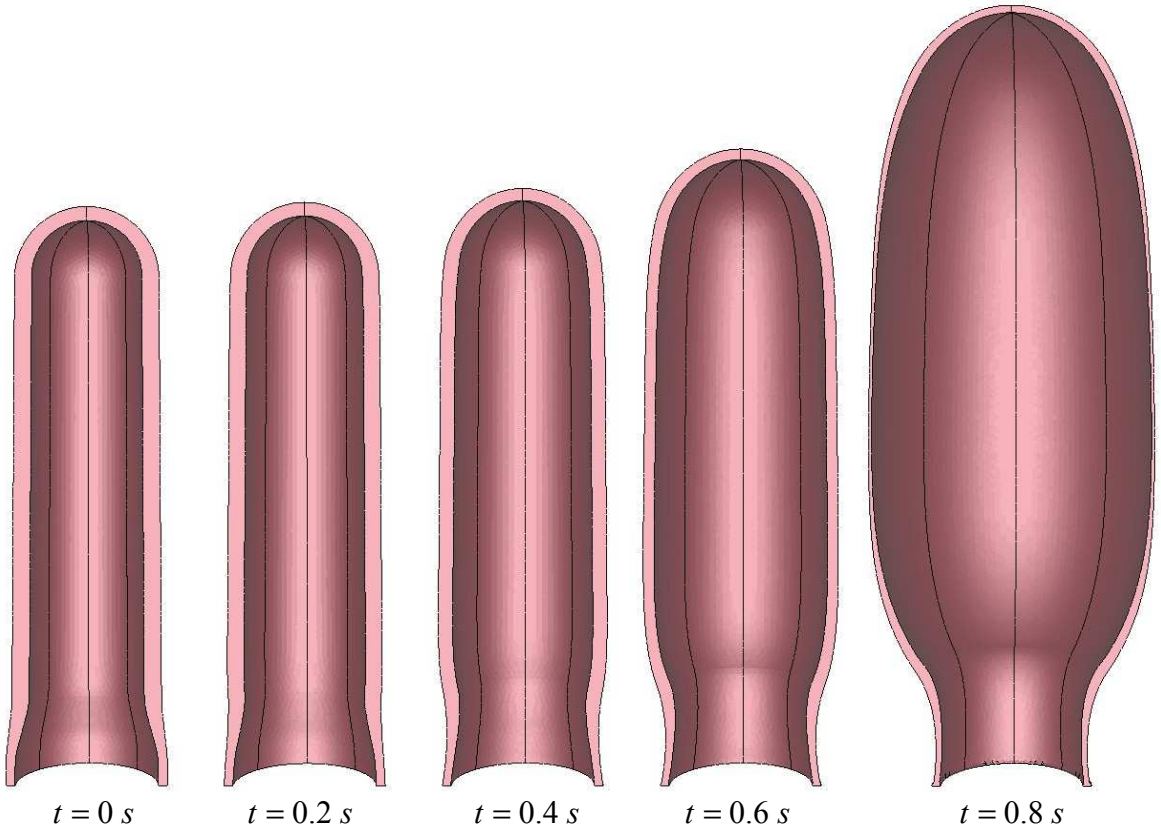

Figure 13 : Intermediate preform free inflation (CPU time = 6 hours).

In a second example, a confined blow molding simulation has been lead. In order to simplify as much as possible and to estimate the numerical parameters bound to the simulation of the process, the constitutive behavior is assumed as a Newtonian law during the blow molding simulation. Indeed, it allowed to reduce efficiently the CPU time.

The mould used is a prototype one developed in the CROMeP (Table 2). It produces 50cl water bottle. As for the tube inflation in part III, just an eighth of the preform has been mesh (fig 14).

Newtonian parameter	$\eta = 0.2\ MPa.s$
Set pressure	Linear $t = 0\ s \rightarrow P = 0\ MPa$ $t = 1\ s \rightarrow P = 1\ MPa$
Preform dimensions	Thickness $= 2.35\ mm$ Internal radius $= 7.6\ mm$ Length $= 68.5\ mm$
Mold dimensions	Internal radius $= 64\ mm$ Length of the print $= 119\ mm$

Table 2 : Calculations parameters.

Figure 14 : Geometries of the preform and the mold.

The followings results (fig. 15) showed that Forge3® is able to model the blow molding process. Indeed, the calculations allowed to estimate with precision the evolution of the shape of the preform during the inflation. Moreover, the software defined perfectly the contact between the mold and the material at any moment of the calculations.

The future works will be to take into account a Mooney-Rivlin law for the P.E.T. material in order to obtain a numerical thickness distribution at the end of the process. This one could be then compared with experimental data. Moreover, the stretch step will be soon added to the model. The final purpose will be to find with the simulation of the stretch blow molding process, the influence on the thickness distribution of parameters like the speed of the rod or the value of the blowing pressure.

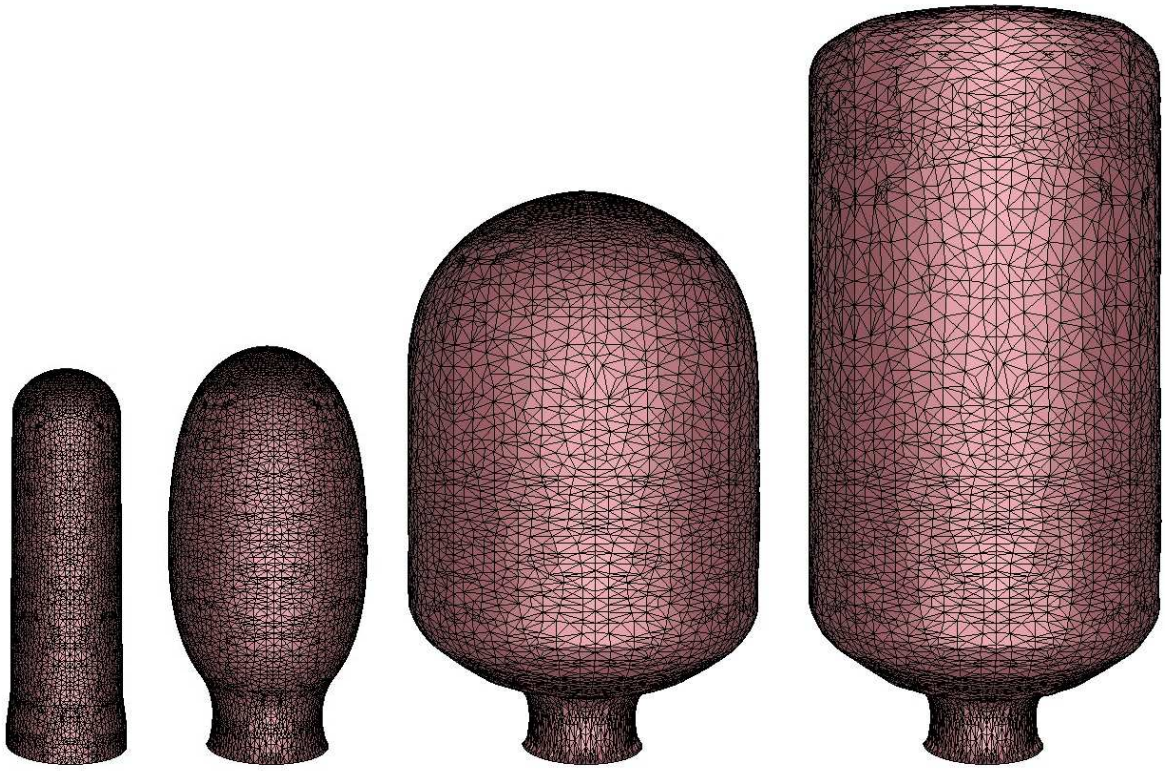

Figure 15 : Intermediate preform blow molding.

V- Conclusion

A numerical thermo-mechanical model has been developed using Forge3® velocity/pressure formulation and tetrahedral elements.
From a thermal point of view, the calculation lead proved that the Rosseland approximation is not adapted to estimate the amount of energy absorbed inside the P.E.T. plastic. Indeed, as the Rosseland conductivity represents less than 2% of the thermal conductivity, the sheet is too much heated on the face submitted to the heat flux. As a consequence, the thermal gradient in the thickness of the material is different from the analytical one. To solve this problem, a complete ray tracing method is being implemented to calculate the irradiative flux value used for the heat balance equation. Both the exchange of energy between the infrared oven and the irradiative surface of the preform, and the amount of radiation energy absorbed inside the material will be thus accurately calculated.
From a mechanical point of view, a Mooney-Rivlin hyperelastic law behavior has been implemented with a complete finite element analytical formulation. In the same way, the model of a plan strain blowing of a tube has been developed in order to validate the calculations. It allowed to validate the implementation did. Future works will be to implement the more complex potential of Edwards-Vilgis, which is more representative of the PET behavior heated up to its glass transition temperature.
Those next developments will enable us to model accurately the complete PET bottles fabrication process, namely, the infrared exchange in the oven and the stretching and blowing step.

Acknowledgements

Nestlé Waters supports this work. Special thanks go to L.G. for the English correction.

References

[EDW1986] S.F. Edwards, T. Vilgis, " The effect of entanglements in rubber elasticity ", Polymer 27 (1986), 483-492.

[DIR1993] R. DiRaddo, A. Garcia-Rejon, " Dynamic modeling of the preform reheating stage in injection blow molding ", Plastic Rubber and composites processing and applications, vol. 20, no 5, 1993.

[GER1973] P. Germain, " Cours de Mécanique des Milieux Continus ", Tome 1, Théorie Générale, Masson et Cie, Editeurs, 1973 (in french).

[GOR2001] E. Gorlier, J.F. Agassant, J.M. Haudin, N.Billon, " Experimental and theoretical study of uniaxial deformation of amorphous poly(ethylene terephthalate) above glass transition temperature ", Plastics, Rubber and Composites, vol. 30, pp 48-55, 2001.

[HAR1996] K. Hartwig, " Simulation of the stretch blow molding process and characterisation of the relevant material behaviour ", Ph. D. Dissertation, RWTH, Aachen, 1996.

[LEB1992] P. Lebaudy, J.M. Saiter, J. Grenet, C. Vautier, " Temperature distribution in poly(ethylene terephtalate) plate undergoing heat treatment ", Diffusion influence : 1, Theoretical approach, Polymer, vol. 33, no 9, 1992

[LIN2002] B. van der Linden, " Radiative heat transfer in glass : the algebraic ray trace method ", PhD, Eindhoven, 2002.

[MAR1997] S. Marie, " Un modèle de parallélisation SPMD pour la simulation des procédés de mise en forme des matériaux ", Ph. D. Thesis, Ecole des Mines de Paris, 1997 (in French).

[MAR2003] Y. Marco, " Caractérisation multi-axiale du comportement et de la micro-structure d'un semi-cristallin : application au cas du P.E.T. ", Thèse de Doctorat en Mécanique, Ecole Normale Supérieure de Cachan, 2003 (in french).

[MEN2000] G.H. Menary, C.G. Armonstrong, R.J. Crawford and J.P. McEvoy, " Modeling of Poly(ethylene terephtalate) in injection stretch blow molding ", Plastics, Rubber and Composites 2000, vol 29, n°7.

[MOD1993] M. Modest, " Radiative heat transfer ", McGraw-Hill, Inc., 1993.

[MON2001] S. Monteix, F. Schmidt, Y. Le Maoult, R. Ben Yedder, R.W. Diraddo, D. Laroche, " Experimental study and numerical simulation of preform or sheet exposed to infrared radiative heating ", Journal of Materials Processing Technology 119 (2001) 90-97.

[ROS1989] D. Rosato, " Blow molding handbook ", Hanser Publishers, 1989.

[SCH1992] F. Schmidt, J.F. Agassant, M. Bellet, G. Denis, " Numerical simulation of polyester stretch-blow molding ", in Numerical methods in industrial forming processes, Balkema, Rotterdam, pp383, 1992.

[SCH2000] F. Schmidt, A. Rodriguez-Villa, J.F. Agassant, M. Bellet, " Analytical models for the inflation of a polymeric tube ", Eur. J. Mech. A/ Solids 19 (2000) 89-104.

[SHE1991] M.D. Shelby, " Effects of infrared lamp temperature and other variable on the reheat rate of PET ", ANTEC'91, 1991.

[VEN1997] G. Venkateswaran, M.R. Cameron, S.A. Jabarin, " Effects of temperature profiles trough preform thickness on the properties of reheat blown PET containers ", ANTEC'97, 1997.

[WAN1998] S. Wang, A. Makinouchi, T. Nakagawa, " 3D viscoplastic FEM simulation of a stretch blow molding process ", International Journal for Numerical Methods in Engineering, vol 48, n°4, pp501-521, 2000.

Nomenclature

ρ	Density	$\underline{\underline{\sigma}}$	Stress tensor
c_p	Specific heat	$\underline{\underline{\sigma}}'$	Extra-stress tensor
T	Temperature	p'	Arbitrary pressure
t	Time	$\underline{\underline{F}}$	Gradient tensor
$\vec{q}$	Density heat flux	$\underline{\underline{B}}$	Left Cauchy Green tensor
$\overrightarrow{q_r}$	Density radiative heat flux	W	Deformation energy
k	Thermal conductivity	C , α	Mooney-Rivlin variables
Ω	Field considered	I_1 , I_2	First two $\underline{\underline{B}}$ invariants
ϕ	Heat flux	$\underline{v}^*$	Virtual velocity
h_{conv}	Convection coefficient	$\underline{S}$	Stress vector
h_{cond}	Conduction coefficient	v	Node speed
T_{ext}	External temperature	b	Bubble speed
T_{front}	Tool temperature	$[H]$	Rigidity matrix
σ_{SB}	Stefan-Boltzmann constant	$[R]$	Residual matrix
k_{ROSS}	Rosseland mean coefficient	p	Pressure
ν	Frequency	N_i	Shape function
κ_ν , κ	Absorption coefficient	v^i	i-th node velocity
B	Planck function	X	Coordinate
$[C]$	Capacity matrix	δ , ε	Permittivity function
$[K]$	Conductivity matrix	R	Internal radius
$[Q]$	Load vector	S	External radius
α_d	Diffusivity		